

# The Coupled Cluster Method in Hamiltonian Lattice Field Theory: SU(2) Glueballs

Andreas Wichmann, Dieter Schütte, Bernard C. Metsch and Vera Wethkamp\*

*Institut für Theoretische Kernphysik  
Nußallee 14–16, D–53115 Bonn  
Germany*

(November 20, 2018)

The glueball spectrum within the Hamiltonian formulation of lattice gauge theory (without fermions) is calculated for the gauge group SU(2) and for two spatial dimensions.

The Hilbert space of gauge-invariant functions of the gauge field is generated by its parallel-transporters on closed paths along the links of the spatial lattice. The coupled cluster method is used to determine the spectrum of the Kogut-Susskind Hamiltonian in a truncated basis. The quality of the description is studied by computing results from various truncations, lattice regularisations and with an improved Hamiltonian.

We find consistency for the mass ratio predictions within a scaling region where we obtain good agreement with standard lattice Monte Carlo results.

## I. INTRODUCTION AND SURVEY

It is the purpose of this paper to present the results of an attempt to compute the spectrum of a lattice gauge field theory within the Hamiltonian formulation. Our computational framework is the coupled cluster method which has been presented and discussed in detail in Ref. [14].

We have applied our method to the lattice version of the SU(2) Yang-Mills theory in two spatial dimensions which is the simplest non-trivial non-abelian lattice gauge field theory. We consider this model whose dynamics is given by a special Kogut-Susskind Hamiltonian as an important test case for controlling the coupled cluster method. Although there is no experiment to compare with, there exist for this model very reliable results for the ground state energy (see Ref. [7,8]) and for glueball masses (see Ref. [18]) which allow a critical test of the coupled cluster predictions.

In the past, several attempts have been made to compute glueball masses within the same model. We mention the light-front approach of van de Sande *et al.* (see Ref. [5]) and the maximal tree approach of Bishop *et al.* (see Ref. [11]).

Calculations similar to ours, i.e. treating the Kogut-Susskind Hamiltonian within the coupled cluster method,

were undertaken by Llewellyn Smith and Watson (see Ref. [12]) and Guo *et al.* (see Ref. [2–4]).

Within the present work we are able to go far beyond the limitations of this earlier work:

- When expanding the characteristic correlation functions within a localized loop basis (see Ref. [14]), we can push the expansion up to the *7th order*.
- We are able to check the validity of the computation of the characteristic coupled cluster matrix elements by comparing *two independent formulations* of the local loop space basis expansion (see Ref. [14,20]).
- We can compare the predictions of *different lattice regularizations* which exist in two spatial dimensions: square, hexagonal and triangular lattice.
- We compute glueballs with *all possible angular momentum quantum numbers* allowed within the lattice formulation, i.e.  $J^P = 0^+, 0^-, 2^+, 2^-, 1^\pm$  for the square lattice and  $J^P = 0^+, 0^-, 3^+, 3^-, 1^\pm, 2^\pm$  for the hexagonal or triangular lattice.
- We also test the quality of our results by comparing to those with an *improved Hamiltonian*.

Taking dimensionless *mass ratios* we observe a good *scaling window* (around  $\beta = 3$  for the non-improved case). Judging the stability of the results within the scaling window by testing the convergence with the order of the coupled cluster expansion, by comparing the predictions of the different lattice regularisations and the inclusion of improvement, we are able to *predict* the spectrum of the energetically low-lying glueballs *within certain errors* (see Fig. 7). Within these errors, our prediction of the glueball spectrum *agrees with that of Teper* (see Ref. [18]). Since our results are very encouraging it is, of course, desirable to extend these computations to more physical models. The SU(2) lattice Yang-Mills theory for  $D = 3+1$  dimensions has been worked out (see Ref. [20]), but the results are too preliminary to be presented. The extension of our model to the SU(3) gauge group is under way (see Ref. [19]). The inclusion of quarks, i.e. the treatment of full QCD, is possible in principle, but technically difficult. First attempts using the coupled cluster

---

\*e-mail: wethkamp@itkp.uni-bonn.de

method for such models exist, but only for the Schwinger model (i.e. the 1+1 dimensional  $U(1)$  case) (see Ref. [6]). Our paper is organized as follows:

Section II defines our computational scheme, especially details of the coupled cluster expansion.

Section III describes the structure of the two local loop space expansions (algebraic versus Clebsch-Gordan methods) and how the computation of the coupled cluster matrix elements is done.

Section IV gives some details of how to project localized wave function on good lattice momentum and angular momentum (only lattice momentum zero is considered within this paper).

Section V describes some calculational details, especially the truncation procedure which is necessary to fix the coupled cluster method.

Section VI presents results for the *vacuum state*. It is shown that within the scaling window the vacuum energy agrees with the value obtained by the Greens function Monte Carlo method (see Ref. [8]) better than within 0.1% showing that the coupled cluster method is thus reliable.

Section VII gives the results for the glueball masses. The stability of the results within the scaling window is shown by testing stability with respect to the order of the coupled cluster expansion (Subsection VII A), with respect to improvement (Subsection VII B) and with respect to the different regularizations (Subsection VII C).

In the Appendix we discuss the different scales in the Hamiltonian and the Lagrangian formulation (see Ref. [9]) and study the possibility to have a *scaling region around*  $\beta = 3$  for our framework.

## II. COMPUTATIONAL SCHEME

Within the Hamiltonian formulation, the computational framework of any lattice Yang-Mills theory is given by the Kogut Susskind theory which has been discussed in detail in Ref. [14]. In summary, the structure is the following: The Kogut Susskind wave functions  $\Psi(U) = \Psi(U_1, \dots, U_N)$  depend on link variables  $U_l$  ( $l = 1, \dots, N$ ) which are elements of the gauge group  $SU(N_c)$ .  $N$  is the number of oriented links in a lattice (with  $d$  spatial dimensions).  $N$  is related to the finite volume chosen. Our many-body technique allows us to perform the final calculations in the infinite volume limit  $N \rightarrow \infty$ . Our concrete calculations are done for the case  $N_c = 2$  and  $d = 2$ .

The idea of the coupled cluster method is to reformulate the eigenvalue problem  $H\Psi = E\Psi$  as equations for the ground state correlation function  $S$  and for the excitation operators  $F$ , following from the ansatzes  $\Psi_0(U) = \exp S(U)$  for the ground state and  $\Psi(U) = F(U) \exp S(U)$  for excited states.

If  $H = 1/(2a)(\sum_{lc} g^2 E_{lc}^2 - 2/g^2 V)$  is the Kogut Susskind Hamiltonian (we use the notations ( $lc$ ) for link-colour

quantum numbers,  $E_{lc}$  for the momentum operators conjugate to  $U_l$  and  $V$  for the plaquette term) this yields the non-linear equation

$$\sum_{lc} (S_{lclc} + S_{lc} S_{lc}) - \frac{2}{g^4} V = \frac{2a}{g^2} E_0 \quad (1)$$

for  $S$  and the linear equation

$$\sum_{lc} (F_{lclc} + 2S_{lc} F_{lc}) = \frac{2a}{g^2} (E - E_0) F \quad (2)$$

for the excitation operators  $F$ . We use the notation that  $f_{lc}$  abbreviates “link variable derivatives” of functions  $f(U)$ :

$$\begin{aligned} f_{lc} &= [E_{lc}, f] \\ f_{lclc} &= [E_{lc}, [E_{lc}, f]]. \end{aligned}$$

This (rigorous) form of the eigenvalue problem manifestly guarantees the correct volume dependencies of both the ground state energy  $E_0$  and the excitation energies  $E - E_0$  (see Ref. [14]).

Within this paper we will consider excitations corresponding to glueballs with arbitrary lattice angular momentum and parity, but with momentum zero. Thus the eigenvalues are interpreted as glueball masses. We may then write

$$\begin{aligned} F &= F_{\sigma}^{k,\nu} = \sum_{\nu} \tilde{\Pi}_{\nu\sigma}^k F_{\text{int}}^{k,\nu} \\ S &= \tilde{\Pi}^0 S_{\text{int}} \end{aligned}$$

where  $\tilde{\Pi}_{\sigma\sigma}^k$  is the projection operator on states with vanishing (lattice) momentum and angular momentum-parity  $k$  (e.g.  $k = J^P = 0^+, 0^-, 2^+, 2^-, 1^{\pm}$  for the square lattice).  $\nu, \sigma$  are magnetic quantum numbers, for more details see Section IV. We abbreviate  $\tilde{\Pi}_{00}^{0^+} = \tilde{\Pi}^0$ .

The essential point of the coupled cluster method is that it can be shown that the functions  $S_{\text{int}}$  and  $F_{\text{int}}$  are *localized* (see Ref. [14]) so that it is plausible to *expand* these intrinsic functions with respect to a localized, gauge invariant, linked, standard basis  $\chi^{\alpha}$  in the form

$$\begin{aligned} S_{\text{int}}(U) &= \sum_{\alpha} S_{\alpha} \chi^{\alpha}(U) \\ F_{\text{int}}^{k,\nu}(U) &= \sum_{\alpha} F_{\alpha}^{k,\nu} \chi^{\alpha}(U) \end{aligned}$$

and to define the approximation to the eigenvalue problem by a *truncation* of this basis.

Introducing the constant function via  $\chi^0 = 1$ , the “plaquette function” by putting  $\tilde{\Pi}_0 \chi^1 = 4V$  and using the strong coupling structure  $\sum_{lc} \chi_{lclc}^{\alpha} = \epsilon_{\alpha} \chi^{\alpha}$  which is true for any convenient basis, the coupled cluster equations (1) and (2) become equations for the coefficients  $S_{\alpha}$  and  $F_{\alpha}^{k,\nu}$ :

$$\begin{aligned} \epsilon_\alpha S_\alpha + \sum_{\beta, \gamma} C_{\alpha,0}^{\beta, \gamma, 0} (k=0^+) S_\gamma S_\beta \\ = \frac{1}{2g^4} \delta_{\alpha 1} + \frac{aE_0}{4Ng^2} \delta_{\alpha 0} \end{aligned} \quad (3)$$

$$\begin{aligned} \epsilon_\alpha F_\alpha^{k, \nu} + 2 \sum_{\beta, \gamma, \nu'} C_{\alpha, \nu'}^{\beta, \gamma, \nu} (k) S_\gamma F_\beta^{k, \nu'} \\ = \frac{2a}{g^2} (E - E_0) F_\alpha^{k, \nu} \end{aligned} \quad (4)$$

Here, the coupled cluster matrix elements  $C_{\alpha, \nu'}^{\beta, \gamma, \nu} (k)$  are given by the following prescription:

Define first numbers  $c_{\alpha u w}^{\beta \gamma}$  which are related to the action  $T(u)$  ( $u \in G_E$ ) of the lattice Euclidean group  $G_E$  (see Section IV for details) on the basis  $\chi^\alpha$  and its products by

$$\chi^\beta T(u) \chi^\gamma = \sum_{\alpha, w \in G_E} c_{\alpha u w}^{\beta \gamma} T(w) \chi^\alpha \quad (5)$$

Here only those cases have to be considered where the functions  $\chi^\beta$  and  $T(u) \chi^\gamma$  have a common link variable, i.e. only a finite number of possible values for the Euclidean group elements  $u, w$  occurs in Eq. (5).

The coupled cluster matrix elements are then related to the matrix elements  $D_{\nu, \nu'}^k (b)$  of the representations of the lattice rotations  $b$  ( $u = (b, \mathbf{a})$ , where  $\mathbf{a}$  = lattice translation, see Section IV) by

$$C_{\alpha, \nu'}^{\beta, \gamma, \nu} (k) = \frac{1}{2} (\epsilon_\alpha - \epsilon_\beta - \epsilon_\gamma) \sum_{\substack{u=(b, \mathbf{a}), \\ w=(b', \mathbf{a}')}} D_{\nu, \nu'}^k (b^{-1} b') c_{\alpha u w}^{\beta \gamma} \quad (6)$$

### III. THE LOOP SPACE BASIS

The basis  $\chi^\alpha$  which we use for our calculations is systematically generated from Eq. (5) in two steps.

In a first step, certain subspaces  $H^{\delta, k}$  of dimension  $m_{\delta, k}$  are generated from geometrically inequivalent plaquette products. The second step then is the construction and the handling of orthogonal basis systems of these subspaces, especially the computation of the coupled cluster matrix elements. This is done in two alternative ways, by algebraic and by Clebsch Gordan techniques.

The subspace  $H^{\delta, k}$  is *generated* from a function  $\Lambda_G^{\delta, k}$  which is given by a linked, standard  $\delta$ -fold plaquette product of the type

$$\begin{aligned} \Lambda_G^{\delta, k} = \chi^1 T(u_2(\delta, k)) \chi^1 \dots T(u_\delta(\delta, k)) \chi^1 \\ k = 1, \dots, n_\delta \end{aligned} \quad (7)$$

where  $u_\lambda(\delta, k)$  ( $\lambda = 2, \dots, \delta$ ) are suitable elements of the lattice Euclidean group. For  $\delta = 0, 1$  we define  $n_0 = n_1 = 1$ ,  $\Lambda_G^{0, 1} = \chi^0$ ,  $\Lambda_G^{1, 1} = \chi^1$ .

The “order” of the functions in the subspace  $H^{\delta, k}$  is defined to be  $\delta$ . In general, the quantum number  $k$  characterizes the different, geometrically independent possibilities for the construction of the plaquette products of the same order whose total number is  $n_\delta$ .

Up to 7th order we have for our two-dimensional  $SU(2)$  case

$n_\delta = 1, 1, 2, 4, 12, 35, 129, 495$  for the square lattice,

$n_\delta = 1, 1, 2, 5, 15, 53, 235, 1125$  for the hexagonal lattice and

$n_\delta = 1, 1, 2, 3, 8, 17, 54, 162$  for the triangular lattice, for  $\delta = 0, \dots, 7$ .

The functions  $\Lambda_G^{\delta, k}$  are characterized by simple loop patterns exemplified up to 4th order in Tables I, II and III. Here, also the dimensions  $m_{\delta, k}$  of the corresponding subspaces  $H^{\delta, k}$  are given.

Each function  $\Lambda_G^{\delta, k}$  ( $\delta, k$  fixed) generates an orthogonal basis  $\chi^{(\delta, k, r)}$ ,  $r = 1, \dots, m_{\delta, k}$ , of  $H^{\delta, k}$ , and taking all quantum numbers  $(\delta, k, r)$  and the limit  $\delta \rightarrow \infty$ , this basis becomes complete for the expansion of localized functions.

There are two ways to define the basis of  $H^{\delta, k}$  explicitly.

#### A. The algebraic method

The idea of this procedure is to act on  $\Lambda_G^{\delta, k}$  with a suitable set of commuting Casimir operators of a lattice gauge group. Hereby, this lattice gauge group  $SU(N_c)^M$  is finite dimensional, where  $M(\delta, k)$  is the number of link variables contained in  $\Lambda_G^{\delta, k}$ .

This yields a generating system for the space  $H^{\delta, k}$  and diagonalizing the corresponding Casimir matrices defines the orthogonal basis. The relation to the generating system allows then to compute also the coefficients  $c_{\alpha u w}^{\beta \gamma}$  (see Ref. [14] for details and examples).

The drawback of this method to construct the basis  $\chi^\alpha = \chi^{(\delta, k, r)}$  is that one has to take care of possible linear dependencies between the generated loop space functions. In previous investigations (see Ref. [12, 2–4, 14]) this problem was solved by exploiting the Cayley Hamilton relationship between matrices. We have used in this connection a much simpler procedure: If a set  $f_1(U), \dots, f_n(U)$  contains only  $m$  ( $m \leq n$ ) independent functions, the matrix  $f_i(U^k)$  ( $i, k = 1, \dots, n$ ) has for suitable *fixed* variables  $(U^1, \dots, U^n)$  exactly the rank  $m$ . Our experience is that statistically chosen variable sets  $(U^1, \dots, U^n) \in SU(2)$  are suitable in this sense. The linear relation between the functions  $f_i$  is then easily constructed and the dependent functions can be eliminated. This works quite well up to the 6th order. For higher orders, however, this method became too unreliable because of increasing numerical errors when checking the linear dependencies in this way.

## B. The Clebsch-Gordan method

Each basis function  $\chi^\alpha$  generated by the algebraic method can be characterized by a set of angular momentum quantum numbers adjoined to a certain plaquette pattern related to the corresponding function  $\Lambda_G^{\delta,k}$ . For the case of a hexagonal lattice, this pattern consists of adjoining a certain angular momentum quantum number  $j_l$  to each link variable occurring in  $\Lambda_G^{\delta,k}$ , the possible values of  $j_l$  being given by simple coupling rules. For the square (see Ref. [14]) or the triangular lattice, also “intermediate” quantum numbers have to be taken into account. This can be systemized by replacing the lattice by a certain “net” containing only three-point vertices and by defining the plaquette pattern within this net. We skip here the description of this net, details can be found in Ref. [20].

The set  $\{j_l\}$  of these quantum numbers defines  $\chi^\alpha = \chi^{\{j_l\}}$  as a well defined function of the link variables  $U_l$  in terms of Clebsch-Gordan coefficients, see Ref. [16,17,15,20]. For convenience, the set  $\{j_l\} = (j_1, j_2, \dots)$  will be assumed to be infinite dimensional by putting  $j_l = 0$  for all links of the net not occurring in the plaquette pattern related to  $\chi^\alpha$ .

This makes it possible to work directly with the orthonormal basis  $\chi^{\{j_l\}}$  and to compute the coupled cluster matrix elements with the help of standard group theoretical methods. Generalizing the notion  $\{j_l\}$  also to non-standard functions, i.e. putting  $T(u)\chi^{\{j_l\}} = \chi^{\{j_l'\}}$ , the essential formula allowing to compute the coefficients  $c_{\alpha uv}^{\gamma\beta}$  via certain  $9j$ -symbols is given by

$$\chi^{\{j_l^1\}}\chi^{\{j_l^2\}} = \sum_{\{j_l^3\}} c^{\chi(\{j_l^1\}, \{j_l^2\}, \{j_l^3\})} \chi^{\{j_l^3\}}, \quad (8)$$

$$c^{\chi(\{j_l^1\}, \{j_l^2\}, \{j_l^3\})} = \prod_{\substack{\text{positively} \\ \text{oriented } l}} \hat{j}_l^1 \hat{j}_l^2 \hat{j}_l^3 \times \prod_v \left\{ \begin{array}{ccc} j_{l(v,1)}^1 & j_{l(v,1)}^2 & j_{l(v,1)}^3 \\ j_{l(v,2)}^1 & j_{l(v,2)}^2 & j_{l(v,2)}^3 \\ j_{l(v,3)}^1 & j_{l(v,3)}^2 & j_{l(v,3)}^3 \end{array} \right\}, \quad (9)$$

where  $\hat{j} = \sqrt{2j+1}$ .

In Eq. (8) the (in each case finite) sum runs only over those sets  $\{j_l^3\}$  which obey for each  $l$  the selection rule  $|j_l^1 - j_l^2| \leq j_l^3 \leq j_l^1 + j_l^2$  and the condition  $j_l^1 \neq 0$  or  $j_l^2 \neq 0$ .

In Eq. (9), we have used the notation  $\{l(v,1), l(v,2), l(v,3)\}$  for the three links  $l$  adjacent to the vertex  $v$ .

For the application of the coupled cluster equation *including truncation* one has to know the *order* of the function  $\chi^{\{j_l\}}$ , i.e. to which subspace  $H^{\delta,k}$  it belongs - the plaquette pattern of  $\{j_l\}$  does not give this uniquely. This order is, however, easily obtained when constructing the basis  $\chi^{\{j_l\}}$  by iterative Clebsch-Gordan coupling, see Ref. [14] for examples.

## IV. THE LATTICE EUCLIDEAN GROUP

Any explicit calculation involves the treatment of the lattice Euclidean group  $G_E$  which consist of translations and rotations,  $G_E = G_T \otimes_s G_R$ , leaving the (infinite) lattice invariant.

### A. Lattice Translations

Translations  $\mathbf{x} \rightarrow \mathbf{x} + \mathbf{a}$  are given by translation vectors

$$\mathbf{a} = a_1 \mathbf{e}_1 + a_2 \mathbf{e}_2$$

where  $\mathbf{e}_1 = \begin{pmatrix} 1 \\ 0 \end{pmatrix}$ . For the other unit vector we have that

$\mathbf{e}_2 = \begin{pmatrix} 0 \\ 1 \end{pmatrix}$  for a square lattice and  $\mathbf{e}_2 = \begin{pmatrix} \cos(\frac{\pi}{3}) \\ \sin(\frac{\pi}{3}) \end{pmatrix}$  for the hexagonal or triangular lattice, respectively.

All distances will be measured in units of the lattice spacing. The numbers  $a_1, a_2$  are then integers which are arbitrary for the square or the triangular lattice and obey a simple restriction for the hexagonal lattice (see Ref. [20]).

### B. Lattice Rotations

General Euclidean transformation are given by a pair  $(b, \mathbf{a})$  mapping  $\mathbf{x} \rightarrow b\mathbf{x} + \mathbf{a}$  where  $b \in G_R$  is a lattice rotation.

For the square lattice, the “point group”  $G_R$  has the eight elements  $(b_0, \dots, b_7)$  which may be written in terms of the following  $2 \times 2$  matrices

$$b_n = \begin{pmatrix} \cos(n\frac{\pi}{4}) & \sin(n\frac{\pi}{4}) \\ -\sin(n\frac{\pi}{4}) & \cos(n\frac{\pi}{4}) \end{pmatrix}$$

$$b_{n+4} = \begin{pmatrix} 0 & 1 \\ 1 & 0 \end{pmatrix} b_n, n = 0, \dots, 3.$$

For the *hexagonal or triangular lattice* the group  $G_R$  has the 12 elements  $(b_0, \dots, b_{11})$  which we write in the form

$$b_n = \begin{pmatrix} \cos(n\frac{\pi}{3}) & \sin(n\frac{\pi}{3}) \\ -\sin(n\frac{\pi}{3}) & \cos(n\frac{\pi}{3}) \end{pmatrix}$$

$$b_{n+6} = \begin{pmatrix} 1 & 0 \\ 0 & -1 \end{pmatrix} b_n, n = 0, \dots, 5.$$

### C. Irreducible Representations

We now list the irreducible representations (irreps) of  $G_R$  (see e.g. Ref. [1]).

For the square lattice (*hexagonal or triangular lattice*) we have 5 (6) inequivalent irreducible representations (irreps)  $D^k$ , 4 one-dimensional irreps labelled

$A_1, A_2, B_1, B_2$  and one (*two*) two-dimensional irreps labelled E ( $E_1, E_2$ ). In the continuum limit, these irreps will correspond to the lowest spins  $0^+, 0^-, 2^+, 2^-$  and  $1^\pm$  ( $0^+, 0^-, 3^+, 3^-, 1^\pm$  and  $2^\pm$ ), respectively. Note that, in the continuum limit, the eigenvalues for the quantum numbers  $J^+$  and  $J^-$  have to be degenerate for  $J \neq 0$  for a rotational invariant Hamiltonian. Explicitly, the irreps read for the one-dimensional cases ( $n = 0, \dots, 7$ ) for the square lattice ( $n=0, \dots, 11$  for the hexagonal or triangular lattice)

$$D^{A_1}(b_n) = 1$$

$$D^{A_2}(b_n) = \det(b_n)$$

$$D^{B_1}(b_n) = (-1)^n \det(b_n)$$

$$D^{B_2}(b_n) = (-1)^n$$

The two-dimensional irreps read for the square case

$$D^E(b_n) = b_n \quad (n = 0, \dots, 7),$$

and for the hexagonal or triangular case

$$D^{E_1}(b_n) = b_n$$

$$D^{E_2}(b_n) = (-1)^n b_n \quad (n = 0, \dots, 11)$$

#### D. Projections on Lattice Momenta and Angular Momenta

The group  $G_E$  acts on the functions  $\chi^{\{j_l\}}$  via

$$T(u)\chi^{\{j_l\}} = \chi^{\{j_{l'}\}} \\ l' = u^{-1}l$$

for  $u \in G_E$ .

This allows to define projection operators on good momentum  $\mathbf{p}$  within the Brillouin zone by

$$\Pi_{\mathbf{p}}^T = \sum_{\mathbf{a}} e^{i\mathbf{p}\mathbf{a}} T(0, \mathbf{a}).$$

States with fixed lattice angular momentum may be constructed by the operators

$$\Pi_{\nu\sigma}^k = N_k \sum_n D_{\nu\sigma}^k(b_n^{-1}) T(b_n, 0), \quad (10)$$

where the normalization factor  $N_k = \dim D^k / |G_R|$  guarantees the projector property

$$\Pi_{\nu\nu}^k \Pi_{\nu\nu}^k = \Pi_{\nu\nu}^k.$$

The index  $\sigma$  in Eq. (10) corresponds to a ‘‘magnetic’’ quantum number since we have

$$T(b)\Pi_{\nu\sigma}^k = \sum_{\sigma'} D_{\sigma,\sigma'}^k(b)\Pi_{\nu\sigma'}^k. \quad (11)$$

Thus for the eigenvalue problem of a rotationally invariant Hamiltonian  $\sigma$  can be fixed, e.g. to  $\sigma = 0$ .

Eq. (11) also shows that the operator  $\Pi_{\nu\sigma}^k$  generates the representation  $D^k$  twice if it is two-dimensional. Thus the index  $\nu$  is not a ‘‘good’’ quantum number, the Hamiltonian will in general mix states with different values of  $\nu$ .

For our concrete calculations we restricted the computation to eigenstates with momentum zero. This simplifies the work because  $\Pi_0^T$  commutes with the operators  $\Pi_{\nu\sigma}^k$ . A basis for the expansion of the correlation functions  $S$  or  $F$  is then generated from the localized basis  $\chi^\alpha$  via

$$\{\tilde{\Pi}_{\nu 0}^k \chi^\alpha = \Pi_{\nu 0}^k \Pi_0^T \chi^\alpha | \alpha \in N, 0 \leq \nu \leq \dim D^k\}. \quad (12)$$

The states of Eq. (12) form an orthogonal basis if the functions  $\chi^\alpha$  are orthogonal and if - for the given  $k$  - states are left out which are projected to zero under  $\tilde{\Pi}_{\nu 0}^k$ . This may occur if the loop space pattern related to  $\chi^\alpha$  is too symmetric, i.e. if this state is invariant under a subgroup of the lattice rotation group. Tables IV, V and VI give a survey on the remaining dimension of the relevant subspaces up to the 7th order. Note that for higher angular momenta only calculations in orders with at least  $\delta \geq 5$  make sense.

#### V. COMPUTATIONAL DETAILS

With the definition of Eq. (12) for the basis expansion of the correlation functions  $S$  and  $F$ , it is straightforward to show the validity of the form Eq. (6) of the coupled cluster matrix elements.

For the numerical study, we have set up a computer program which organized efficiently the handling of the loop space and of the lattice Euclidean group. For the computation of the coupled cluster matrix element, we used up to 6th order both the algebraic and the Clebsch Gordan method. We found a perfect agreement which was a comforting assurance of the validity of our computational methods. Details are described in Ref. [20].

For the concrete calculations, we still have to define a truncation prescription. For the results presented below, we follow the proposal of Guo *et al.* (see Ref. [2–4]) which yields actually the simplest set of equations. In this case one puts in the order  $\delta$

$$c_{\alpha_3, u w}^{\alpha_1, \alpha_2} = 0 \quad \text{for} \quad \delta(\chi^{\alpha_1}) + \delta(\chi^{\alpha_2}) > \delta. \quad (13)$$

Since the expansion of the function  $S$  starts with  $\delta = 1$ , our calculations go up to 8th order if the expansion of the correlation functions is pushed to 7th order, as we do within this work.

We have also studied alternative truncations (see Ref. [20]), but we could not find any prescription which was better than Eq. (13).

#### VI. RESULTS FOR THE GROUND STATE

It is a special feature of the Hamiltonian formulation that it provides both the energy and the wave function of the vacuum state which is the ground state of the Hamiltonian.

Standard lattice Monte Carlo calculations do not give results for the vacuum energy density. There exist, however, computations within the strong coupling expansion (see Ref. [7]) and very reliable Green's function Monte Carlo results (see Ref. [8]).

In Figure 1 we compare our coupled cluster results up to 8th order to the results of the other methods. As coupling variable we use the standard expression  $\beta = 4/g^2$ . We see that we obtain excellent results (better than 0.1%) in our scaling region ( $\beta \approx 3$ , see below), we have a good quality and convergence up to  $\beta \approx 4$ , but our method breaks down for large  $\beta$  where the Green's function Monte Carlo is still valid.

An important feature of our results is that the validity of the coupled cluster method clearly goes beyond the range of the strong coupling expansion which breaks down at  $\beta \approx 3$ . (Our figure gives the result of the 18th order of strong coupling perturbation theory!) We consider this improvement as a necessary condition for obtaining continuum limit physics.

We should stress that the determination of the vacuum operator  $S(U)$  - by solving Eq. (3) iteratively - turns out to be much simpler and faster than that of the excitation operator  $F(U)$ . Thus we do not see any special difficulty with the fact that the Hamiltonian formulation also involves the determination of the vacuum state. The coupled cluster formulation deals with this problem apparently quite effectively.

In this sense our framework seems to be quite orthogonal to the light front formulation which is based on the assumption that the simplicity of the vacuum could be helpful for the determination of the spectrum.

## VII. THE GLUEBALL SPECTRUM

The eigenvalues of the solutions of Eq. (4) have the interpretation of (approximate) glueball masses with angular-momentum  $J^P = k$ .

### A. Results on the square lattice

An example of the convergence of the lowest  $0^+$  glueball mass up to the 8th order of the coupled cluster expansion is given in Fig. 2 (upper figure). We see that there is perfect agreement with Hamer's results of the strong coupling expansion (see Ref. [7]) up to  $\beta \approx 2$  which breaks down for larger  $\beta$ . Also Hamer's ESCE method (see Ref. [7]) becomes apparently unreliable for  $\beta \geq 3$ .

Obviously, we are able to estimate in the region  $\beta \approx 3$  the value of the glueball mass within errors.

The problem is whether this region of couplings contains already continuum physics. This we judge from the occurrence of an approximate scaling window for mass ratios.

In Fig. 3 (upper figure) we present mass ratios of the different lowest  $J^P$  states of the square lattice relative to the mass of the  $0^+$  state in 8th order. As an example of the convergence with the order we give in Fig. 4 for the three highest orders the mass ratios of the  $2^-$  state versus the  $0^+$  state. We compare our data with the scaling window results of Teper (see Ref. [18]). As an example of mass ratios of higher excitations we show in Fig. 5 that of the  $0^{+*}$  and the  $2^{+*}$  state, because here a comparison with Teper is also possible.

We assume the scaling window to be at  $\beta \approx 3$ . This allows us to estimate the glueball spectrum within certain errors by comparing the prediction of the 7th and 8th order at  $\beta = 3$ , see Table VII.

Also included are the predictions of the improved Hamiltonian (see Subsection VII B) and of alternative lattices (see Subsection VII C).

For the  $0^-$  sector we have to remark that because the glueball in question lies in the continuum of two (lowest)  $0^+$  glueball states the results are not very reliable. This can be seen having a look on the wave functions of this states. In the  $0^-$  sector extending the calculations from 6th to 7th and 8th order a new state occurs (see Fig. 6). In the strong coupling limit ( $\beta = 0$ ) it has an eigenvalue of twice the eigenvalue of the  $0^+$  glueball and its wave function is exactly the product of two glueball excitation operators: the glueball excitation  $F$  is given by the product of two plaquettes (*two-cluster state*):

$$F_{0^+}(\beta = 0) = \square \quad , 7\text{th order}$$

$$F_{0^-}(\beta = 0) = \square \square \quad , 7\text{th order} .$$

As is the strong coupling limit, the scaling region ( $\beta = 3$ ) is dominated by *two-cluster states*:

$$F_{0^-}(\beta = 3.0) : \begin{array}{l} \square \square + \square \square + \square \square + \square \square \\ 20.25\% + 10.67\% + 10.57\% + 5.86\% \\ + \square \square + \square \square + \text{rest} \\ 4.11\% + 4.02\% + 44.52\% \end{array} , 8\text{th order} .$$

This feature of the wave functions appears in the whole  $0^-$  sector and also in the  $1^\pm$  sector for the  $1^{\pm*}$  state.

The quality of the result on the square lattice is now tested by comparing to other computational schemes yielding equivalent descriptions in the continuum limit.

### B. Results with improvement

The definition of an improved action (see Ref. [10]) or an improved Hamiltonian (see Ref. [13]) is not unique. Within our work, we have studied the simplest choice, namely a tadpole improvement of the plaquette part of the Hamiltonian. This is given by the following prescriptions (see Ref. [10]).

Replace

$$\text{tr}(\square) \rightarrow \frac{1}{u_0^4} \left( \frac{5}{3} \text{tr}(\square) - \frac{1}{6u_0^2} \text{tr}(\square) \right)$$

where  $u_0$  is related to the vacuum expectation value of the plaquette via

$$u_0^4 = \langle \psi_0 | \frac{1}{N_c} \text{tr}(\square) | \psi_0 \rangle$$

which, in turn, may be computed using the Feynman-Hellmann formula

$$\langle 0 | \text{tr}(\square) | 0 \rangle = \frac{d}{d\lambda} \langle 0 | H + \lambda \text{tr}(\square) | 0 \rangle \Big|_{\lambda=0}.$$

Improvement changes the scales of  $\beta$ . Our results show that the scaling region is shifted from  $\beta \approx 3$  to  $\beta \approx 1.7$ , but the prediction of mass ratios should not change.

Repeating the computation of the ground state with improvement we find similar convergence properties as before. The plaquette vacuum expectation value turns out to be  $u_0 \approx 0.84$  for  $\beta \approx 2$ .

As an example for the quality of the convergence with improvement we show in Fig. 2 (lower figure) the behaviour of the lowest  $0^+$  glueball mass and in Fig. 3 (lower figure) the structure of the scaling window which appear to be improved, indeed.

Taking the predictions of 7th and 8th order at  $\beta = 1.7$  we obtain for the glueball ratios the numbers given in Table VII which show a remarkable agreement to the non-improved results.

### C. Results for alternative lattices

We have also computed the ground state and the glueball spectrum for the hexagonal and for the triangular lattice. Using the “geometrical” rescalings

$$\begin{aligned} \beta &\rightarrow \frac{2}{3}\beta \\ E_0 &\rightarrow \frac{2}{3}E_0 \end{aligned}$$

we find in both cases perfect agreement of the vacuum energy to that for the square lattice.

Using the same rescaling for the glueball masses, we observe again an approximate scaling region for  $\beta \approx 3$ . Since for these new lattices, the scaling quality for the  $2^+$  glueball is better than that for the  $0^+$  case, the numbers presented in Table VII were estimated of the mass ratios of the different  $J^P$  states relative to the  $2^+$  glueball and then rescaled to the  $0^+$  state.

For both new lattices, we find a new prediction for the  $3^+$  and  $3^-$  glueball which turns out to be approximately degenerate in the scaling region, as it should be.

For the triangular lattice, because of level crossings between the lowest and the first excited state in the  $1^\pm$  and in the  $3^-$  sector we find results which differ from other lattices.

Like on the square lattice also on the hexagonal and the triangular lattice the  $0^-$  sector is dominated by two-cluster states. In addition the two-cluster states influence also the first and second excitations in the  $1^\pm$  and the  $3^\pm$  sector on the hexagonal lattice.

Nevertheless we perform a “final” estimate of the glueball spectrum in units of the  $0^+$  glueball by calculating mean values of the numbers of different orders and different lattices of Table VII, yielding the predictions of Fig. 7 (left values). The errors are deviations of the mean values. We do not take into account read off errors.

We see that, indeed, we obtain predictions quite consistent with the Monte Carlo results of Teper, see Ref. [18] (middle and right values in Fig. 7).

## ACKNOWLEDGEMENTS

D.S. acknowledges useful discussions with Chris Hamer, Gastao Krein, Helmut Kröger and Xiang Luo.

## APPENDIX

Within this Appendix we comment on the question whether it is possible to have a scaling region  $\beta \approx 3$  if this region starts only with  $\beta \gg 4$  within the standard lattice Monte Carlo method (see Ref. [18]).

The point is that a comparison to our Hamiltonian results involves a rescaling of the standard “Euclidean” coupling  $g_E$  relative to the Hamiltonian coupling  $g$ . For  $g \rightarrow 0$  this is given by (see Ref. [9])

$$\beta_E = \beta + .077 + O(g^2).$$

There is also rescaling of the Euclidean masses  $M_E$  relative to the Hamiltonian masses  $M$  (“velocity of light correction”)

$$M_E = (1 + 0.084g^2 + O(g^4))M.$$

However, one cannot expect that these formulae hold for  $\beta \approx 3$  because the difference between  $\beta_E$  and  $\beta$  becomes very large in the strong coupling regime itself. The strong coupling expansions are completely different in the Euclidean and Hamiltonian formalisms: the Euclidean expansion has a logarithmic singularity for  $\beta_E = 0$  which is not present in the Hamiltonian framework.

The rigorous relation between  $\beta_E$  and  $\beta$  is not known. Consequently for  $\beta \approx 3$  a direct comparison of masses to Teper’s results appears not to be possible.

---

[1] S.L. Altmann, C.J. Bradley, Rev. of Modern Physics, **37** (1965) 33.

[2] Q. Chen, S. Guo, X. Fang and W. Zheng, Phys. Rev. D **50** (1994) 3564.

[3] Q. Chen, X. Luo, S. Guo and X. Fang, Phys. Lett. B **348** (1995) 560 [hep-ph/9502235].

[4] S. Guo, Q. Chen and L. Li, Phys. Rev. D **49** (1994) 507.

[5] S. Dalley and B. van de Sande, "Precision study of large-N Yang-Mills theory in 2+1 dimensions," Phys. Rev. D **63** (2001) 076004 [hep-lat/0010082].

[6] X. Fang, D. Schütte, V. Wethkamp and A. Wichmann, Phys. Rev. D **64** (2001) 014501.

[7] C. J. Hamer, J. Oitmaa and W. H. Zheng, Phys. Rev. D **45** (1992) 4652.

[8] C. J. Hamer, M. Sheppard, W. Zheng and D. Schütte, Phys. Rev. D **54** (1996) 2395 [hep-th/9511179].

[9] C. J. Hamer, Phys. Rev. D **53** (1996) 7316.

[10] P. Lepage, Nucl. Phys. Proc. Suppl. **60A** (1998) 267 [hep-lat/9707026].

[11] N. E. Ligterink, N. R. Walet and R. F. Bishop, Annals Phys. **284** (2000) 215 [hep-lat/0001028].

[12] C. H. Llewellyn Smith and N. J. Watson, Phys. Lett. B **302** (1993) 463 [hep-lat/9212025].

[13] X. Luo, S. Guo, H. Kröger and D. Schütte, Phys. Rev. D **59** (1999) 034503 [hep-lat/9804029].

[14] D. Schütte, W. Zheng and C. J. Hamer, Phys. Rev. D **55** (1997) 2974 [hep-lat/9603026].

[15] D. Schütte, A. Wichmann and V. Wethkamp, Int. J. Mod. Phys. B **15** (2001) 1732.

[16] D. Robson and D. M. Webber, Z. Phys. C **15** (1982) 199.

[17] A. C. Irving, T. E. Preece and C. J. Hamer, Nucl. Phys. B **270** (1986) 536.

[18] M. J. Teper, Phys. Rev. D **59** (1999) 014512 [hep-lat/9804008].

[19] V. Wethkamp, work in progress.

[20] A. Wichmann, Dissertation, TK-01-03, ITKP University of Bonn (2001) <http://www.itkp.uni-bonn.de/~wichmann/dissertation.html>

## TABLES

TABLE I. Construction of the Loop Space Basis: The functions  $\Lambda_G^{\delta,k}$  generating  $m_{\delta,k}$ -dimensional subspaces are characterized by simple loop patterns. Altogether we have 84 basis elements in the order  $\delta \leq 4$  for the square lattice.

$\Lambda_G^{\delta,k}$	$m_{\delta,k}$	$\Lambda_G^{\delta,k}$	$m_{\delta,k}$
$\Lambda_G^{0,1} = 1$	1	$\Lambda_G^{4,1} = \text{■}$	1
		$\Lambda_G^{4,2} = \text{■□}$	2
$\Lambda_G^{1,1} = \text{□}$	1	$\Lambda_G^{4,3} = \text{■□□}$	7
		$\Lambda_G^{4,4} = \text{■□□□}$	3
$\Lambda_G^{2,1} = \text{■□}$	1	$\Lambda_G^{4,5} = \text{■□□□□}$	5
$\Lambda_G^{2,2} = \text{□□}$	2	$\Lambda_G^{4,6} = \text{■□□□}$	6
		$\Lambda_G^{4,7} = \text{■□□□□}$	4
$\Lambda_G^{3,1} = \text{■□□}$	1	$\Lambda_G^{4,8} = \text{■□□□□□}$	9
$\Lambda_G^{3,2} = \text{■□□□}$	2	$\Lambda_G^{4,9} = \text{■□□□□□□}$	9
$\Lambda_G^{3,3} = \text{■□□□□}$	4	$\Lambda_G^{4,10} = \text{■□□□□□□□}$	10
$\Lambda_G^{3,4} = \text{■□□□□□}$	3	$\Lambda_G^{4,11} = \text{■□□□□□□□□}$	7
		$\Lambda_G^{4,12} = \text{■□□□□□□□□□}$	6
			84

TABLE II. Construction of the Loop Space Basis: The functions  $\Lambda_G^{\delta,k}$  generating  $m_{\delta,k}$ -dimensional subspaces are characterized by simple loop patterns. Altogether we have 94 basis elements in the order  $\delta \leq 4$  for the hexagonal lattice.

$\Lambda_G^{\delta,k}$	$m_{\delta,k}$	$\Lambda_G^{\delta,k}$	$m_{\delta,k}$
$\Lambda_G^{0,1} = 1$	1	$\Lambda_G^{4,1} = \text{⦿}$	1
$\Lambda_G^{1,1} = \text{○}$	1	$\Lambda_G^{4,2} = \text{⦿○}$	2
$\Lambda_G^{2,1} = \text{⦿}$	1	$\Lambda_G^{4,3} = \text{⦿○⦿}$	6
$\Lambda_G^{2,2} = \text{○○}$	2	$\Lambda_G^{4,4} = \text{⦿○⦿○}$	5
$\Lambda_G^{3,1} = \text{⦿}$	1	$\Lambda_G^{4,5} = \text{⦿○⦿○}$	3
$\Lambda_G^{3,2} = \text{⦿○}$	2	$\Lambda_G^{4,6} = \text{⦿○⦿○}$	5
$\Lambda_G^{3,3} = \text{⦿○⦿}$	3	$\Lambda_G^{4,7} = \text{⦿○⦿○}$	4
$\Lambda_G^{3,4} = \text{⦿○⦿○}$	3	$\Lambda_G^{4,8} = \text{⦿○⦿○}$	4
$\Lambda_G^{3,5} = \text{⦿○⦿○}$	3	$\Lambda_G^{4,9} = \text{⦿○⦿○}$	6
		$\Lambda_G^{4,10} = \text{⦿○⦿○}$	10
		$\Lambda_G^{4,11} = \text{⦿○⦿○}$	7
		$\Lambda_G^{4,12} = \text{⦿○⦿○}$	6
		$\Lambda_G^{4,13} = \text{⦿○⦿○}$	8
		$\Lambda_G^{4,14} = \text{⦿○⦿○}$	4
		$\Lambda_G^{4,15} = \text{⦿○⦿○}$	6
			94

TABLE III. Construction of the Loop Space Basis: The functions  $\Lambda_G^{\delta,k}$  generating  $m_{\delta,k}$ -dimensional subspaces are characterized by simple loop patterns. Altogether we have 58 basis elements in the order  $\delta \leq 4$  for the triangular lattice.

$\Lambda_G^{\delta,k}$	$m_{\delta,k}$	$\Lambda_G^{\delta,k}$	$m_{\delta,k}$
$\Lambda_G^{0,1} = 1$	1	$\Lambda_G^{4,1} = \blacktriangle$	1
$\Lambda_G^{1,1} = \triangle$	1	$\Lambda_G^{4,2} = \blacktriangle$	2
$\Lambda_G^{2,1} = \triangle$	1	$\Lambda_G^{4,3} = \blacktriangle$	7
$\Lambda_G^{2,2} = \triangle$	2	$\Lambda_G^{4,4} = \blacktriangle$	3
		$\Lambda_G^{4,5} = \blacktriangle$	6
		$\Lambda_G^{4,6} = \blacktriangle$	9
		$\Lambda_G^{4,7} = \blacktriangle$	10
		$\Lambda_G^{4,8} = \blacktriangle$	8
			58

TABLE IV. Lattice Angular Momenta: The number of basis elements  $\chi^\alpha$  for the different spins on the square lattice.

order	$\delta \leq 0$	$\delta \leq 1$	$\delta \leq 2$	$\delta \leq 3$	$\delta \leq 4$	$\delta \leq 5$	$\delta \leq 6$	$\delta \leq 7$
$\chi^\alpha$	1	2	5	15	84	557	4942	47751
$\Pi^{0+} \chi$	1	2	5	15	84	557	4942	47751
$\Pi^{0-} \chi$	0	0	0	1	31	377	4220	45132
$\Pi^{2+} \chi$	0	0	2	8	65	497	4759	47073
$\Pi^{2-} \chi$	0	0	0	4	42	425	4386	45790
$\Pi^{1\pm} \chi$	0	0	0	8	79	874	8841	92340

TABLE V. Lattice Angular Momenta: The number of basis elements  $\chi^\alpha$  for the different spins on the hexagonal lattice.

order	$\delta \leq 0$	$\delta \leq 1$	$\delta \leq 2$	$\delta \leq 3$	$\delta \leq 4$	$\delta \leq 5$	$\delta \leq 6$	$\delta \leq 7$
$\chi$	1	2	5	17	94	677	6430	67036
$\Pi^{0+} \chi$	1	2	5	17	94	677	6430	67036
$\Pi^{0-} \chi$	0	0	0	1	35	464	5613	63947
$\Pi^{3+} \chi$	0	0	0	4	43	512	5728	64573
$\Pi^{3-} \chi$	0	0	0	6	52	573	5989	65854
$\Pi^{1\pm} \chi$	0	0	0	8	91	1078	11691	130381
$\Pi^{2\pm} \chi$	0	0	2	12	120	1128	12008	130924

TABLE VI. Lattice Angular Momenta: The number of basis elements  $\chi^\alpha$  for the different spins on the triangular lattice.

order	$\delta \leq 0$	$\delta \leq 1$	$\delta \leq 2$	$\delta \leq 3$	$\delta \leq 4$	$\delta \leq 5$	$\delta \leq 6$	$\delta \leq 7$
$\chi$	1	2	5	12	58	341	2958	27885
$\Pi^{0+} \chi$	1	2	5	12	58	341	2958	27885
$\Pi^{0-} \chi$	0	0	0	1	21	249	2601	26857
$\Pi^{3+} \chi$	0	0	0	1	22	250	2603	26859
$\Pi^{3-} \chi$	0	1	2	9	41	324	2807	27734
$\Pi^{1\pm} \chi$	0	0	0	7	56	562	5393	54550
$\Pi^{2\pm} \chi$	0	0	2	9	71	577	5538	54695

TABLE VII. The mass ratios of various glueball states  $J^P$  relative to the  $0^+$  state for the square, the square improved, the hexagonal and the triangular lattice in 7th and 8th order in the scaling region.

$J^P$	square		square impr.		hexagonal		triangular	
	$\beta = 3$	$\beta = 3$	$\beta = 1.7$	$\beta = 1.7$	$\beta = 3$	$\beta = 3$	$\beta = 3$	$\beta = 3$
	$\delta = 7$	$\delta = 8$						
$0^+$	1	1	1	1	1	1	1	1
$0^{+*}$	–	1.47	1.43	1.41	1.51	1.42	–	1.76
$0^-$	1.78 <sup>a</sup>	2.00 <sup>a</sup>	1.82 <sup>a</sup>	2.01 <sup>a</sup>	1.65 <sup>a</sup>	2.00 <sup>a</sup>	2.13 <sup>a</sup>	2.26 <sup>a</sup>
$0^{-*}$	2.01 <sup>a</sup>	2.06 <sup>a</sup>	2.06 <sup>a</sup>	2.07 <sup>a</sup>	2.08 <sup>a</sup>	2.15 <sup>a</sup>	2.18 <sup>a</sup>	2.32 <sup>a</sup>
$0^{-**}$	2.30 <sup>a</sup>	2.20 <sup>a</sup>	2.34 <sup>a</sup>	2.23 <sup>a</sup>	2.25 <sup>a</sup>	2.20 <sup>a</sup>	2.53 <sup>a</sup>	2.53 <sup>a</sup>
$1^\pm$	2.11	2.10	2.14	2.10	2.17	2.15	2.07 <sup>b</sup>	2.04 <sup>b</sup>
$1^{\pm*}$	2.23	2.22 <sup>a</sup>	2.27	2.25	2.26	2.17 <sup>a</sup>	2.29 <sup>b</sup>	2.12 <sup>b</sup>
$1^{\pm**}$	2.27	2.23	2.30	2.26	2.26	2.19 <sup>a</sup>	2.39	2.35
$2^+$	1.56	1.61	1.57	1.60				
$2^{+*}$	1.77	1.87	1.78	1.83				
$2^{+**}$	1.78	–	1.82	–				
$2^-$	1.68	1.66	1.69	1.66				
$2^{-*}$	1.77	–	1.81	–				
$2^{-**}$	2.11	–	2.08	–				
$2^\pm$					1.60	1.62	1.66	1.65
$2^{\pm*}$					1.65	1.83	1.97	1.99
$2^{\pm**}$					1.65	1.96	2.03	2.05
$3^+$					2.05	2.05	2.20	2.27
$3^{+*}$					2.26	2.16 <sup>a</sup>	2.55	2.52
$3^{+**}$					2.31	2.18 <sup>a</sup>	2.63	2.61
$3^-$					2.06	2.08	1.69 <sup>b</sup>	1.69 <sup>b</sup>
$3^{-*}$					2.27	2.52 <sup>a</sup>	2.09 <sup>b</sup>	1.97 <sup>b</sup>
$3^{-**}$					2.29	2.19 <sup>a</sup>	2.23	2.21

<sup>a</sup>predominantly 2-cluster states

<sup>b</sup>level crossing

FIGURES

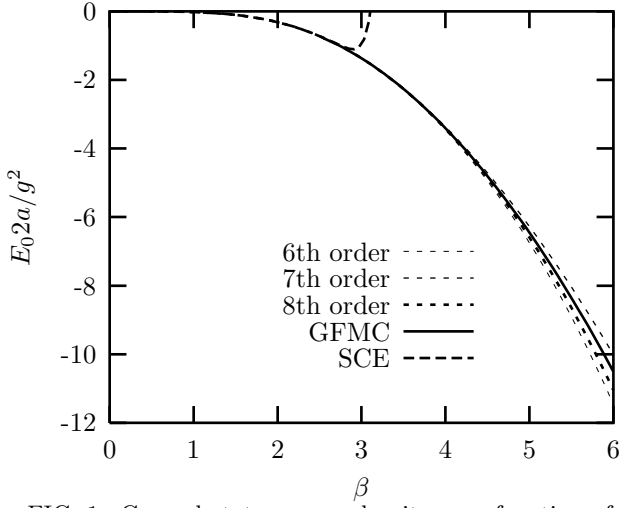


FIG. 1. Ground state energy density as a function of the inverse coupling  $\beta = \frac{4}{g^2}$  up to 8th order. For comparison: Strong coupling expansion SCE [7] and Green's function Monte-Carlo GFMC method [8].

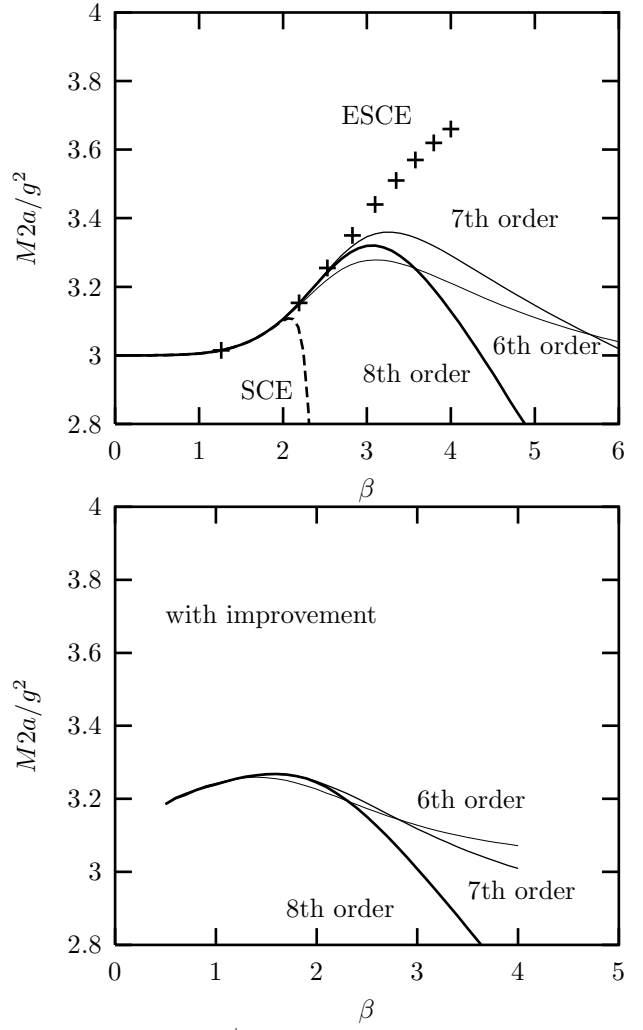


FIG. 2. Excited  $0^+$  state energy as a function of the inverse coupling  $\beta = \frac{4}{g^2}$  up to 8th order without and with improvement. For comparison: Strong coupling expansion SCE and Extrapolation of the strong coupling series ESCE with Shafer and integrated differential approximants [7].

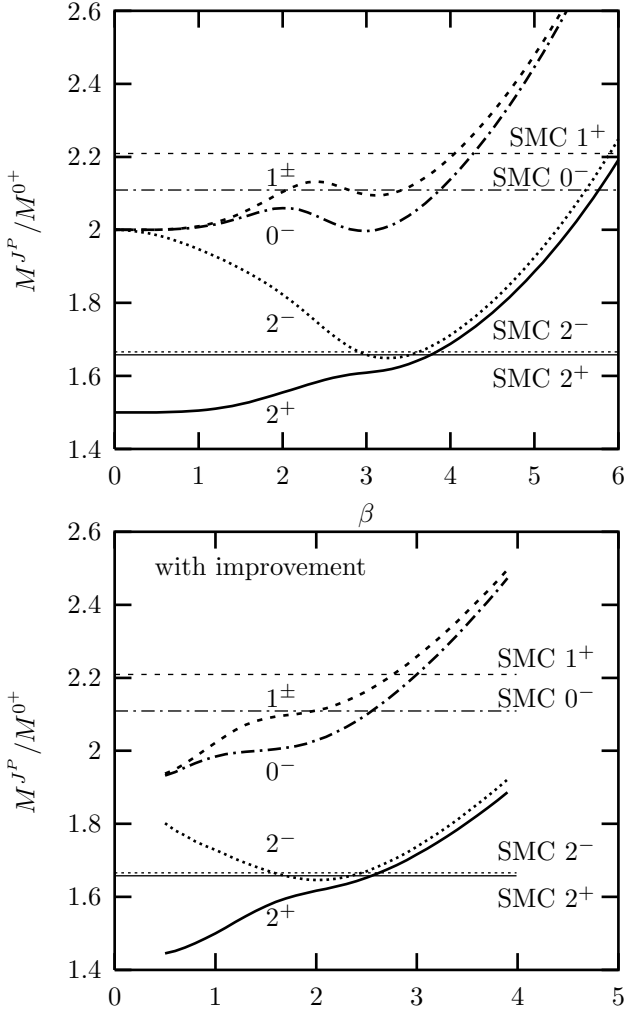


FIG. 3. Mass ratios of the  $J^P = 0^-$ ,  $J^P = 2^+$ ,  $J^P = 2^-$  and the  $J^P = 1^\pm$  state relative to the  $0^+$  state as a function of the inverse coupling  $\beta = \frac{4}{g^2}$  in 8th order without and with improvement. For comparison: Standard Monte Carlo SMC results [18] for  $\xi = 1$  (only scaling window result).  $\xi$  is the anisotropic factor  $\xi = \frac{a_s}{a_t}$ ,  $a_{s(t)}$  = lattice spacing in space (time) direction.

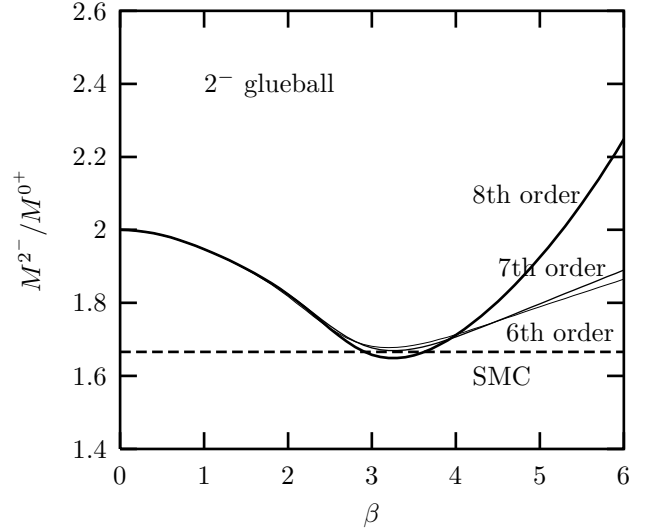


FIG. 4. Mass ratios of the  $J^P = 2^-$  state relative to the  $0^+$  state as a function of the inverse coupling  $\beta = \frac{4}{g^2}$  in 6th, 7th and 8th order to show the convergence with the order. For comparison: Standard Monte Carlo SMC results [18] for  $\xi = 1$  (only scaling window result).  $\xi$  is the anisotropic factor  $\xi = \frac{a_s}{a_t}$ ,  $a_{s(t)}$  = lattice spacing in space (time) direction.

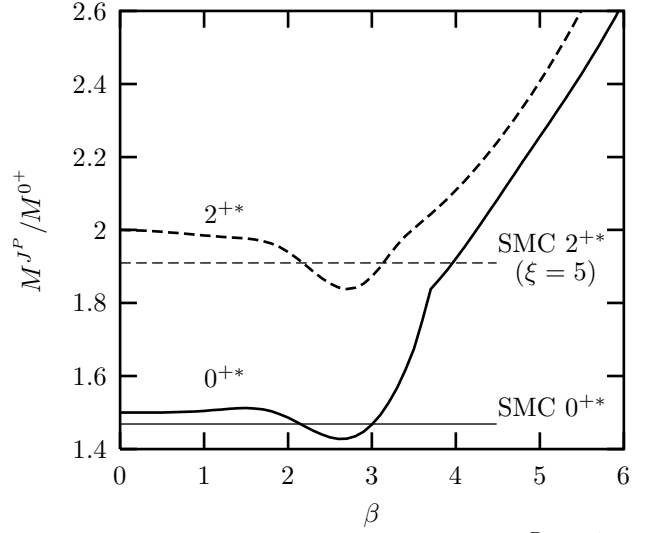


FIG. 5. Mass ratios of the first excitations  $J^P = 0^{+*}$  and  $J^P = 2^{+*}$  glueball states in 8th order. For comparison: Standard Monte Carlo SMC results [18] for  $\xi = 1$  (only scaling window result).  $\xi$  is the anisotropic factor  $\xi = \frac{a_s}{a_t}$ ,  $a_{s(t)}$  = lattice spacing in space (time) direction.

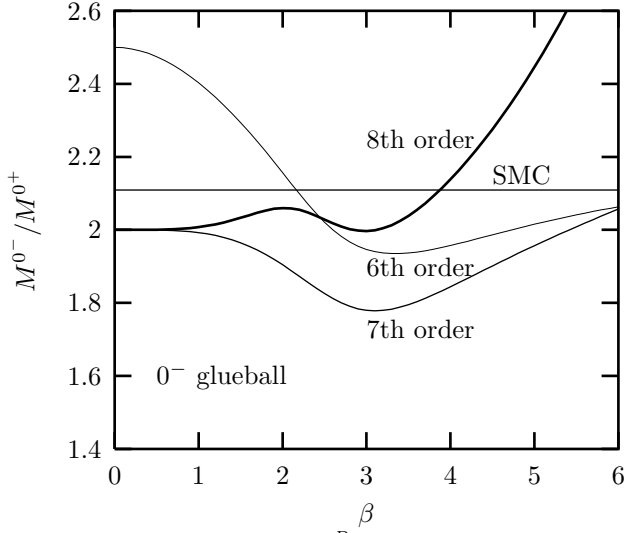


FIG. 6. Mass ratios of the  $J^P = 0^-$  state relative to the  $0^+$  state as a function of the inverse coupling  $\beta = \frac{4}{g^2}$  in 6th, 7th and 8th order. This sector is dominated by 2-cluster states. For comparison: Standard Monte Carlo SMC results [18] for  $\xi = 1$  (only scaling window result).  $\xi$  is the anisotropic factor  $\xi = \frac{a_s}{a_t}$ ,  $a_{s(t)}$  = lattice spacing in space (time) direction.

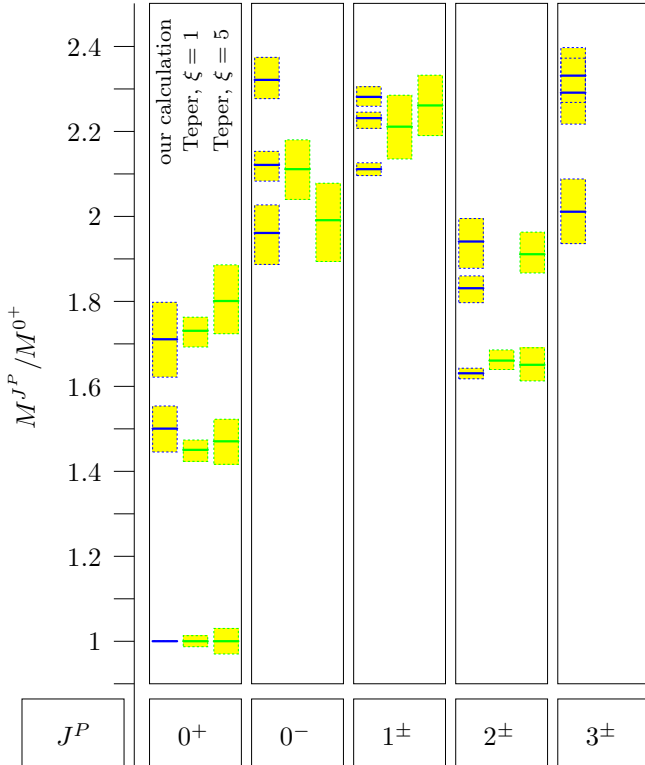


FIG. 7. Final estimate of the glueball spectrum in units of the  $0^+$  glueball. The bars in the left column are mean values of the numbers in Table VII. The shaded area reflects the estimated error. For comparison: Standard Monte Carlo SMC results [18] for  $\xi = 1$  in the middle column and for  $\xi = 5$  in the right column, where  $\xi$  is the anisotropic factor  $\xi = \frac{a_s}{a_t}$ , with  $a_{s(t)}$  = lattice spacing in space (time) direction.